Dye/Peroxalate Aggregated Nanoparticles with Enhanced and Tunable Chemiluminescence for Biomedical Imaging of Hydrogen Peroxide

Yong-Deok Lee,[†,‡] Chang-Keun Lim,[†] Ajay Singh,[†,§] Joonseok Koh,[§] Jungahn Kim,[‡] Ick Chan Kwon,[†] and Sehoon Kim[†,*]

[†]Center for Theragnosis, Korea Institute of Science and Technology, 39-1 Hawolgok-dong, Seongbuk-gu, Seoul 136-791, Korea, [‡]Department of Chemistry, Kyung Hee University, Seoul 130-701, Korea, and [§]Department of Textile Engineering, Konkuk University, Seoul 143-701, Korea

ABSTRACT Hydrogen peroxide (H_2O_2) is an endogenous molecule that plays diverse physiological and pathological roles in living systems. Here we report multimolecule integrated nanoprobes with the enhanced chemiluminescence (CL) response to H_2O_2 that is produced in cells and *in vivo*. This approach is based on the nanoscopic coaggregation of a dye exhibiting aggregation-enhanced fluorescence (AEF) with a H_2O_2-responsive peroxalate that can convert chemical reaction energy into electronic excitation. The coaggregated CL nanoparticles (FPOA NPs) with an average size of ~20 nm were formulated by aqueous self-assembly of a ternary mixture of a surfactant (Pluronic F-127) and concentrated hydrophobic dye/peroxalte payloads. Spectroscopic studies manifest that FPOA NPs as a reagent-concentrated nanoreactor possess the signal enhancement effect by AEF, as well as the optimized efficiencies for H_2O_2 peroxalate reaction and subsequent intraparticle energy transfer to the dye aggregates, to yield greatly enhanced CL generation with a prolonged lifetime. It is shown that the enhanced CL signal thereby is capable of detecting intracellular H_2O_2 overproduced during immune response. We also demonstrate that the densely integrated nature of FPOA NPs facilitates further intraparticle CL energy transfer to a low-energy dopant to red shift the spectrum toward the biologically more transparent optical window, which enables the high-sensitivity *in vivo* visualization of H_2O_2 associated with early stage inflammation.

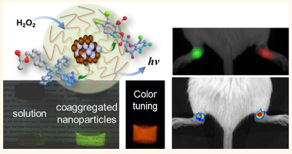

KEYWORDS: aggregation-enhanced fluorescence · peroxalate-based chemiluminescence · multimolecule integrated nanoparticles · hydrogen peroxide · biomedical imaging · inflammation · immune response

Hydrogen peroxide, one of the biologically relevant reactive oxygen species (ROS), has recently been shown to be a major messenger molecule in various redox-dependent cellular signaling transductions.[1] It is also known that its abnormal overproduction is implicated in the progress of inflammation by causing oxidative damage.[2] Therefore, sensitive visualization of the low level of H_2O_2 in cells and *in vivo* is of great importance not only for fundamental studies to understand its role in cellular processes but also for early diagnosis of inflammatory diseases. Among several detection modalities, chemiluminescence (CL) has been well exploited as a contrast signal for high-sensitivity imaging of H_2O_2.[3] Since CL is the emission of light as the result of a chemical reaction without photoexcitation, it offers ultrahigh sensitivity with no noise of photoexcited autofluorescence from the background.[4,5] Nonenzymatic peroxalate-based CL (POCL) reaction has potentially been adopted for the sensitive and selective *in vivo* imaging of H_2O_2 by integrating all reactants needed (peroxalate and dye molecules) in a form of water-dispersed colloids that act as a nanoreactor.[6−9] Figure 1a represents the POCL reaction occurring in the reactant-integrated nanoreactor, where the input of H_2O_2 oxidizes peroxalates (**1**) to produce an electronically excited 1,2-dioxetanedione intermediate (**2**) that subsequently transfers its energy to the coloaded emitting dyes to generate fluorescence by purely chemical excitation.

Recently, we have demonstrated that colloidal POCL nanoreactors can show the enhanced CL sensitivity toward H_2O_2 when concentrated with highly reactive peroxalates.[9] However, the nanoreactor approach has an inherent limitation in that the local concentration of dyes coloaded in the nanoreactor is quite limited to a low level to prevent the typical quenching of molecular fluorescence at high concentration or in the aggregated state.[10] The inevitably low loading of emitting dyes results in a limited

* Address correspondence to sehoonkim@kist.re.kr.

Received for review April 4, 2012 and accepted July 1, 2012.

Published online July 02, 2012
10.1021/nn3014905

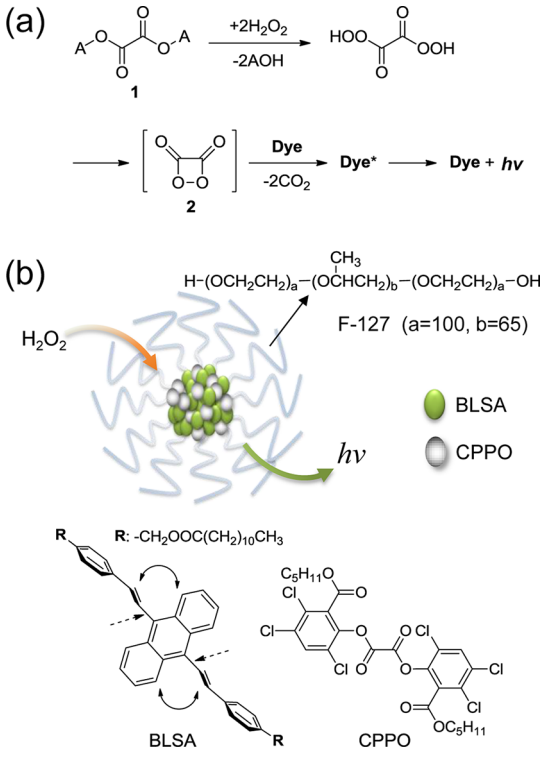

Figure 1. (a) Simplified POCL reaction scheme. (b) Schematic representation of coaggregated nanoparticles (FPOA NPs) and chemical structures of the constituents. In the structure of BLSA, the hydrogens inducing internal steric hindrance and the distorted bonds thereby are indicated by solid and dotted arrows, respectively.

emission output from the peroxalate-concentrated nanoreactor. Since this limitation arises from using common "concentration quenching" dyes, it can be overcome by employing molecules whose fluorescence is not quenched but rather enhanced in the solid state. Solid-state fluorescence, induced or enhanced by chromophoric aggregation, is a unique phenomenon occurring in a special class of molecules that, in most cases, have nonplanar geometries with torsional freedom in the isolated solution state.[11−26] Conceptually, fluorescence output from individual nanoparticles is proportional to a product of loaded dye density and fluorescence efficiency at the loading density. The aggregation-enhanced fluorescence (AEF) allows for high-density loading of dyes in the nanoparticle matrix while keeping their fluorescing capability. Therefore, it is anticipated that this beneficial feature of AEF can enhance the CL brightness of peroxalate-concentrated nanoreactors by further concentrating them with AEF-active dyes as a coloaded emitting component. Nanoparticles concentrated with AEF-active dyes offer another benefit of efficient intraparticle AEF energy transfer when codoped with a low-energy acceptor.[22,23] This advantageous feature would provide a simple way of tuning the CL color into the longer-wavelength optical window, which is advantageous for *in vivo* imaging.

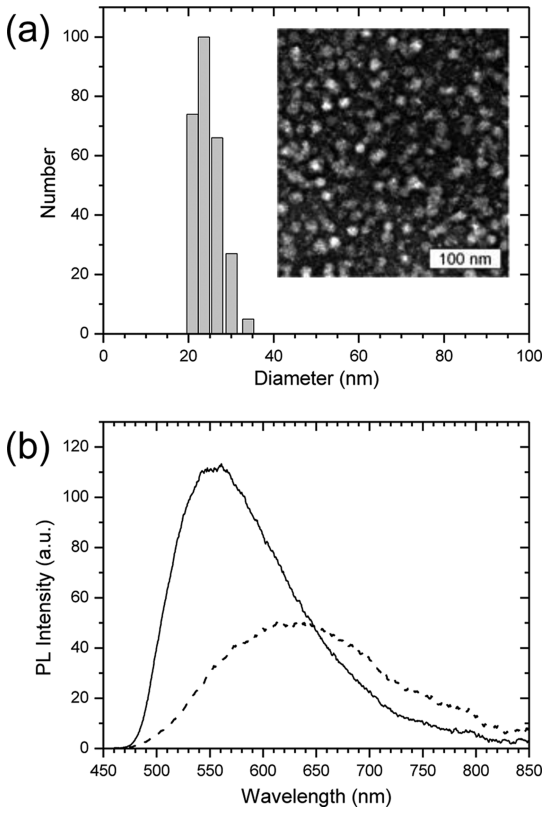

Figure 2. (a) Number-averaged hydrodynamic size distribution and TEM image (inset) of FPOA NPs. (b) PL spectra of water-dispersed FPOA NPs (solid line) and FPOA solution in THF (dashed line).

In order to prove this concept, that is, dual concentration of the nanoreactor with peroxalates and AEF-active dyes for enhancing the nanoparticulate CL, we designed and prepared an aqueous formulation of densely integrated composite nanoparticles (FPOA NPs) based on a biocompatible polymeric surfactant, Pluronic F-127. As shown in Figure 1b, the hydrophobic interior is concentrated with both bis[3,4,6-trichloro-2-(pentyloxycarbonyl)phenyl] oxalate (CPPO) as a highly reactive peroxalate and a 9,10-distyrylanthracene derivative (BLSA) as a green-emitting AEF-active dye. Here we present the AEF-motivated enhancement of POCL signal from the BLSA/CPPO aggregated FPOA NPs, along with the efficient intraparticle CL energy transfer to a low-energy dopant to tune the spectrum toward the biologically more transparent longer-wavelength window. We also demonstrate potential use of the enhanced and tunable nanoparticulate POCL for sensitive imaging of endogenously produced H_2O_2 in cells and *in vivo*.

RESULTS AND DISCUSSION

As an AEF-active dye, we designed and synthesized a green-emitting 9,10-distyrylanthracene derivative (BLSA, see Scheme S1 in the Supporting Information). 9,10-Distyrylanthracene derivatives are a class of AEF-active molecules with a distorted geometry,[19,20] and

their strong solid-state fluorescence has been utilized for bioimaging applications in a form of dye-concentrated nanoparticles.[21−23] BLSA is a strongly green fluorescent solid and showed typical AEF characteristics when comparatively examined with a THF solution and a stable water dispersion of nanoaggregates (see Figure S1 in the Supporting Information). When excited at 412 nm, the photoluminescence (PL) emission is weak in solution ($\lambda_{max.PL}$ = 607 nm, Φ_f = 0.09), whereas it is intensified and hypsochromically shifted by the formation of nanoaggregates ($\lambda_{max.PL}$ = 578 nm, Φ_f = 0.67). In contrast to fluorescence enhancement, the absorbance of BLSA in solution ($\lambda_{max.abs}$ = 412 nm, ε_{max} = 11 400 M^{-1} cm^{-1}) showed a hypochromic effect with no band shift, by aggregation ($\lambda_{max.abs}$ = 412 nm, ε_{max} = 7300 M^{-1} cm^{-1}). No notable sign of H- or J-aggregation was observed, implying that loose molecular stacking (neither closely packed nor well-ordered) within the nanoaggregated structure minimizes the intermolecular fluorescence quenching interaction. This peculiar AEF behavior comes from the distorted π-conjugation framework, as represented by the structure of BLSA in Figure 1.[19,20] Free torsional motion of the isolated BLSA framework in solution promotes fluorescence quenching, whereas the restricted motion in the aggregated state leads to a substantial increase in the fluorescence efficiency.

To incorporate the signal-enhancing feature of AEF into a peroxalate-concentrated CL nanoreactor, a water dispersion of dye/peroxalate aggregated Pluronic nanoparticles (FPOA NPs) was formulated with excess loading of BLSA and CPPO. FPOA NPs were simply fabricated by two steps: (1) homogeneous mixing of Pluronic F-127, CPPO, and BLSA in a methylene chloride solution in a weight ratio of 20:0.5:1; and (2) subsequently adding water to the dried ternary mixture. During the latter step, homogeneously dispersed colloids were spontaneously formed in water by self-assembly behavior of a polymeric amphiphile (F-127). As determined by dynamic light scattering (DLS), the obtained colloids have a number-weighted hydrodynamic size of 24.5 ± 3.1 nm (Figure 2a). The transmission electron microscopic (TEM) image manifests that the dispersed colloids are spherical nanoparticles with an average diameter of 17.3 ± 2.1 nm (the inset of Figure 2a). No apparent precipitates were observed in the dispersion, suggesting that the water-insoluble components (CPPO and BLSA) were fully embedded in the hydrophobic interior of the self-assembled nanostructure of F-127. The colloidal size of FPOA NPs was stably maintained with time in the aqueous dispersion, suggesting that the coaggregated nanostructure is robust without notable leakage of hydrophobic payloads (see Figure S2 in the Supporting Information).

FPOA NPs exhibited intense green emission upon photoexcitation, characteristic of the BLSA aggregates.

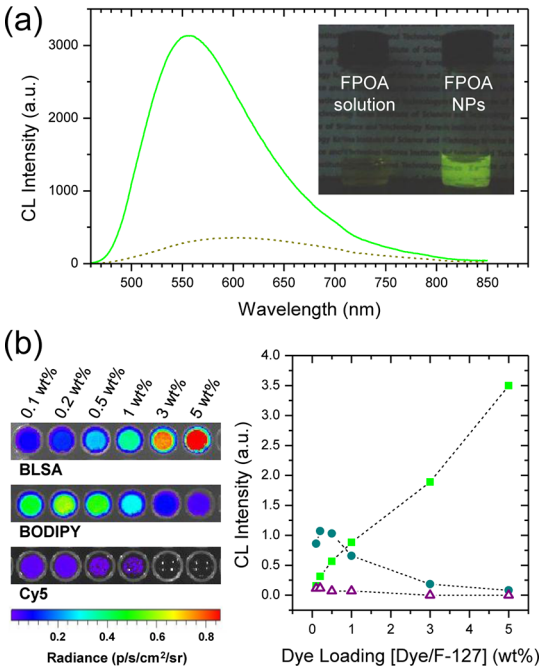

Figure 3. (a) CL spectra of water-dispersed FPOA NPs (solid line) and FPOA solution in THF (dashed line), taken at 10 s after addition of H_2O_2 (0.17 M). The inset is a photograph of the generated CL. (b) CL emission output from CPPO/F-127 nanoparticles entrapping a varying amount of dye (BLSA, BODIPY, or Cy5) whose loading is indicated in wt % with respect to F-127. An IVIS Spectrum imaging system was used to take spectrally unfiltered CL images (left), from which the CL intensities (square, BLSA; circle, BODIPY; triangle, Cy5) were estimated and plotted as a function of dye loading (right).

As shown in Figure 2b, the PL spectrum of FPOA NPs ($\lambda_{max.PL}$ = 553 nm) was blue-shifted compared to that of BLSA-alone nanoaggregates ($\lambda_{max.PL}$ = 578 nm). This hypsochromic shift is attributable to a large population of coaggregating CPPO that may disturb the stacking between BLSA molecules to limit the planarization and thus shorten the effective π-conjugation length. When the dried ternary mixture (F-127/CPPO/BLSA) of the same composition was dissolved in THF (FPOA solution) instead of being dispersed in water, its PL showed a bathochromic shift with an intensity reduction ($\lambda_{max.PL}$ = 630 nm), similar to the pure BLSA solution in THF. Under the given condition (the same composition and the same excitation at 430 nm), FPOA NPs emitted 1.5-fold enhanced PL over FPOA solution, by the formation of nanoparticles. Accordingly, all of the spectral features of FPOA NPs evidence that the embedded BLSA molecules aggregate in the composite particle matrix at the given loading content, to turn on the aggregation-induced enhancement of fluorescence signal.

The effect of intraparticle dye/peroxalate co-condensation on the CL enhancement was examined comparatively between FPOA NPs and FPOA solution. Upon addition of excess H_2O_2 (1 M, 0.2 mL) to the mixtures (1 mL), luminescence generation was

observed from both FPOA NPs and solution samples without photoexcitation, suggesting that the combination of BLSA and CPPO is a good luminescent pair for the POCL reaction. As shown in the CL spectra (Figure 3a), characteristic spectral features of BLSA were observed from the nanoparticulate and solution states ($\lambda_{max.CL}$ = 556 and 603 nm for FPOA NPs and FPOA solution, respectively). At 10 s after addition of H_2O_2, FPOA NPs showed intense CL emission that is 6.3-fold enhanced over that of FPOA solution (Figure 3a). The CL output from FPOA NPs was so strong as to be seen vividly by naked eye under room light, unlike a dim emission from FPOA solution (the inset of Figure 3a). The CL enhancement by aggregation is much greater than that for PL (Figure 2b), suggesting that, in addition to the AEF effect, localization of reactants in the nanoreactor facilitates each CL reaction step in Figure 1a due to the resulting high local concentrations. It was found that the CL generation was weakened with increasing time interval between the particle preparation and H_2O_2 addition, attributable to the degradation of reactive CPPO by hydrolysis (see Figure S3 in the Supporting Information).[27] However, the marginal CL stability of FPOA NPs is considered to be acceptable because most imaging experiments are completed within minutes.

To assess the AEF effect on the CL enhancement, the BLSA composition in FPOA NPs was varied in a range (0.5−5 wt % with respect to F-127) where stable nanoparticle dispersions are obtained in water. It was observed that the initial CL signal (measured at 10 s after addition of H_2O_2) was increased by raising the BLSA loading (Figure 3b), as expected from the unique AEF property. The linear increase in the CL output without any quenching effect evidently indicates the aggregation-induced enhancement effect on emission efficiency. This behavior is directly opposed to a concentration quenching behavior of common hydrophobic dyes, as examined with a green-emitting boron dipyrromethene dye (BODIPY; see Scheme S2 in the Supporting Information) and a near-infrared-emitting cyanine dye (Cy5) that were loaded in the F-127/CPPO composite nanoparticles instead of BLSA. As shown in Figure 3b, the CL output from the common dye-loaded nanoparticles drops significantly with increasing dye content, due to the intermolecular quenching interaction at high local concentration. Importantly, FPOA NPs with 5 wt % BLSA exhibited significantly enhanced CL emission compared to the Cy5-doped FPOC NPs that were developed for *in vivo* CL imaging in our previous work[9] (19 times intenser in the initial CL signal, Figure 3b). The CL quantum yield (ϕ_{CL}) of FPOA NPs, estimated from the total CL emission integrated over time, is 4.4 × 10^{-3} einsteins/mol, that is, ~6 times higher than the value for FPOC NPs that are concentrated only with CPPO (see Figure S4 in the Supporting Information), affirming the validity of our strategy for enhancing the CL generation through the AEF-based multimolecule integration.

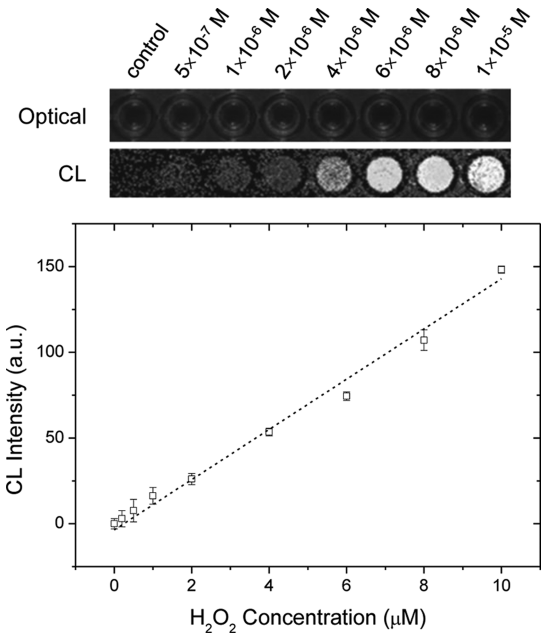

Figure 4. Optical and CL images of FPOA NPs in the presence of low-level H_2O_2 (top, captured with Kodak Image Station), and a correlation between the amount of H_2O_2 and the CL intensity, estimated from the CL images in triplicate (bottom).

Dye/peroxalate aggregation influenced not only CL characteristics but also kinetics of luminescence generation. In the presence of excess H_2O_2 (0.17 M), CL emissions from both FPOA NPs and FPOA solution follow a simple pseudo-first-order kinetic profile[27] (see Figure S5a in the Supporting Information). By formation of the coaggregated nanoparticles, FPOA NPs showed the rise and decay kinetic rates (k_r = 1.2 × 10^{-1} s^{-1} and k_d = 1.0 × 10^{-3} s^{-1}) that were slowed down compared to those of FPOA solution (k_r = 2.1 s^{-1} and k_d = 5.8 × 10^{-3} s^{-1}). It is speculated that the depletion of CPPO by reaction with H_2O_2 (the putative rate-limiting step[27]) might be significantly slowed because the contact with H_2O_2 is limited in the coaggregated nanoparticles. As a result, FPOA NPs have a much longer CL lifetime ($T_{3/4}$ = 23 min, defined as time required for emission of three-quarters of the total luminescence[28]) than FPOA solution ($T_{3/4}$ = 4.5 min; see Figure S5b in the Supporting Information). This indicates that the intensified nanoparticulate CL, with an initial enhancement factor of 6.3, can be emitted for a prolonged period of time. Consequently, it was found that the total luminescence (integrated over time) from the nanointegrated FPOA NPs is further enhanced over FPOA solution by a factor of 55.

The enhanced CL emission might have a practical importance in that it allows high-sensitivity detection of endogenous H_2O_2 that exists at low concentration in biological objects. Figure 4 shows the *in vitro* imaging of CL generated from FPOA NPs under the condition of

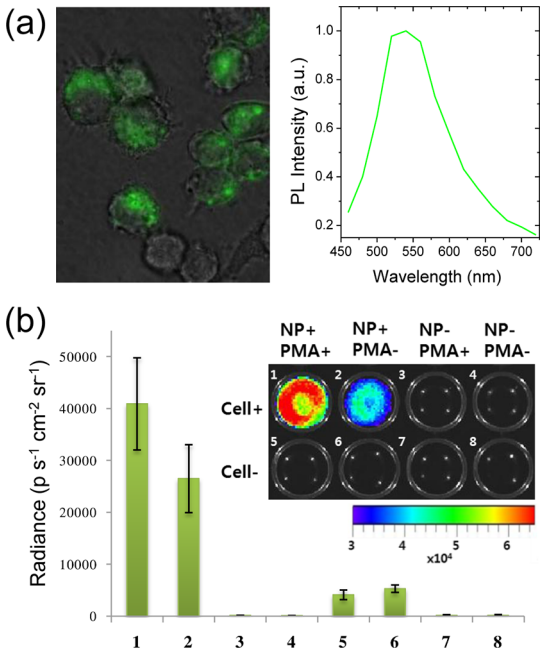

Figure 5. Imaging of PMA-stimulated H_2O_2 production in RAW264.7 macrophages labeled with FPOA NPs. (a) Overlay of PL and transmission images (left) and intracellular PL spectrum (right), acquired with a Nuance multispectral imaging system. (b) Representative image (inset) and quantification of CL emission intensity from experimental groups 1−8 (n = 4) with or without nanoparticles, cells, and PMA stimulation, as indicated in the inset.

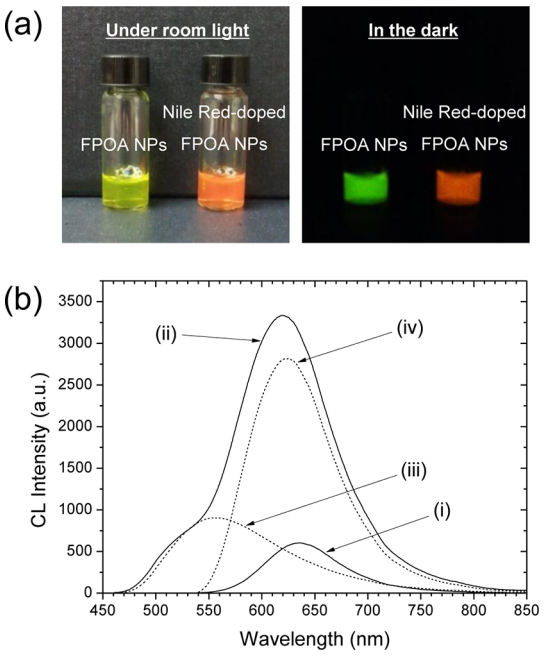

Figure 6. (a) CL emission from FPOA NPs with and without doping of Nile Red, generated by the input of H_2O_2. True-color views were taken with a general-purpose digital camera under room light and in the dark. (b) CL spectra of CPPO/F-127 nanoparticles entrapping (i) 0.02 wt % Nile Red and (ii) 0.02 wt % Nile Red/5 wt % BLSA with respect to F-127. The composite spectrum of the Nile Red-doped FPOA NPs (ii) was deconvoluted into contributions from BLSA (iii) and Nile Red (iv).

low-level H_2O_2, where the concentration down to 10^{-7} M could be reliably detected with a common-use CCD system for fluorescence imaging. This detection limit is close to the normal *in vivo* concentration of H_2O_2 ($\sim 10^{-7}$ M),[1] suggesting that FPOA NPs can detect an abnormal rise of the H_2O_2 level in biological objects. Moreover, the CL intensity showed a linear correlation with the concentration of H_2O_2, allowing for the analytical quantification of H_2O_2. It should be noted that ultra-high-sensitivity detector systems are generally needed for the analytical detection of CL since its signal level is inherently very low compared to PL, particularly in the presence of low-concentration analytes.[9] Therefore, the high detectability of FPOA NPs, attained with a general-purpose CCD, shows the validity of AEF-active dye/peroxalate integration for the CL enhancement.

We next evaluated whether FPOA NPs can be used to label cells and to detect intracellular H_2O_2 produced at low levels upon physiological stimulation. For this, we studied H_2O_2-mediated immune response by macrophages where H_2O_2 is produced as a killing agent for the engulfed pathogens. As a model cell line, we chose RAW264.7 macrophages that are known to produce low micromolar levels of H_2O_2 upon stimulation with phorbol myristate acetate (PMA).[29,30] RAW264.7 cells incubated with FPOA NPs for 10 min at 37 °C displayed strong intracellular PL signals with a characteristic spectral feature of the BLSA aggregates (Figure 5a). This indicates that the Pluronic-surfaced coaggregated nanoparticles are avidly taken up by cells to allow for intracellular H_2O_2 imaging. To examine the H_2O_2-responsive CL generation from the labeled cells, luminescence imaging without photoexcitation was done with various experimental groups by using a high-sensitivity imaging system. As shown in Figure 5b, significant CL signals were only observed from the sample wells containing RAW264.7 cells labeled with FPOA NPs. Even without immune stimulation, the labeled cells showed low but noticeable levels of CL (group 2), implying the high sensitivity of FPOA NPs that can detect low levels of intracellular H_2O_2 inherently present under normal physiological conditions. Upon stimulation with PMA to induce an immune response, a significant signal increase was observed (group 1), suggesting that the enhanced CL from FPOA NPs can sensitively visualize endogenous production of H_2O_2 under conditions of immune signaling.

The BLSA-concentrated structure of FPOA NPs offers another opportunity of facile CL energy harvesting into a low-energy photon when doped with a secondary energy acceptor. As shown in Figure 6a, the CL color of FPOA NPs was readily tuned from green to red by doping only 0.4 wt % Nile Red relative to BLSA. This indicates that the CL energy transfer is efficient owing to close proximity of the donor/acceptor pair within the same nanoparticulate space. The obtained CL spectrum is a composite of the quenched emission

from the BLSA aggregates and the amplified contribution from the acceptor Nile Red (Figure 6b). In comparison to the CL from undoped FPOA NPs, it is estimated that 81% of BLSA emission is quenched by intraparticle energy transfer to Nile Red (see Figure S6 in the Supporting Information). Importantly, the CL emission from Nile Red was amplified 5.2 times by colocalization with excess BLSA within FPOA NPs, when compared to that from nanoparticles containing the corresponding amounts of Nile Red and CPPO without BLSA. This suggests that, in addition to direct energy transfer (1,2-dioxetanedione → Nile Red), indirect cascade CL energy funneling (1,2-dioxetanedione → BLSA → Nile Red) is significant for the chemical excitation of Nile Red. The high efficiency of energy transfer (81%) and 5.2-fold low-energy photon amplification evidence that densely loaded BLSA molecules forming AEF-active aggregates act as an efficient energy-transferring bridge by providing an optimal condition for intraparticle collection and harvest of photon energies generated by the POCL reaction.

Longer-wavelength tuning of the CL emission is advantageous for *in vivo* applications since increasing the wavelength of light toward the near-infrared (NIR) decreases the photon-limiting interferences in biological tissues (scattering and absorption) and thus increases the light penetration.[31,32] As discussed above, the optical down-conversion by doping Nile Red significantly increases NIR components in the CL emission of FPOA NPs, which would enhance the *in vivo* detectability. To demonstrate this, we attempted diagnostic *in vivo* imaging for the early stage inflammation and evaluated spectral dependence on the CL sensitivity toward H_2O_2 produced in deep tissues (Figure 7). As an inflammatory disease model, arthritis was induced in mouse ankle joints by injecting lipopolysaccharide (LPS). CL images were taken after intra-articular administration of Nile Red-doped or undoped FPOA NPs at 48 h after LPS injection (an early stage of inflammation[33]). Spectral imaging manifested that the *in vivo* CL spectra of undoped and Nile Red-doped FPOA NPs well reflect the corresponding green and red emissions observed *in vitro* (Figure 7a), suggesting that the multimolecule integrated nanostructures are stably maintained in the given bodily condition. To quantify and compare the total emission from each experimental condition, photons throughout the whole spectral window were collected without using any optical filter. As shown in the obtained unfiltered CL images (Figure 7b), efficient signals were only detected from the LPS-treated inflamed joints, along with negligible emission from the LPS-negative normal side (see Figure S7 in the Supporting Information). The fairly high inflamed-to-normal contrasts achieved with both green and red emissions imply that FPOA NPs have potential for early diagnosis of inflammation with the enhanced CL response that allows for the sensitive imaging of low-level H_2O_2. Importantly, the red-shifted CL emission showed

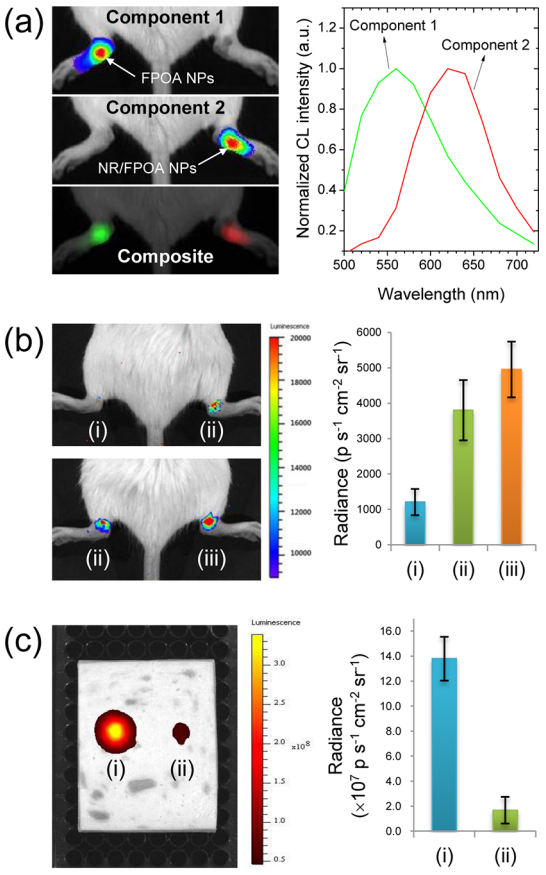

Figure 7. *In vivo* CL imaging of the LPS-induced arthritis model with undoped (green luminescent) or Nile Red-doped (red luminescent) FPOA NPs, using an IVIS Spectrum imaging system. (a) Spectrally unmixed component and composite images (left) and spectral profiles used to unmix images (right). Green and red FPOA NPs were injected into each inflamed ankle just before imaging. (b) Spectrally unfiltered images (left) and quantification (right) of CL emission intensity from experimental groups (n = 4): (i) preinjected PBS + green FPOA NPs, (ii) preinjected LPS + green FPOA NPs, and (iii) preinjected LPS + red FPOA NPs. (c) Spectrally unfiltered image (left) and quantification (right) of CL emissions from red FPOA NPs and NIR-emissive FPOC NPs[9] through the biological tissue (7 mm thick chicken ham, n = 4).

further improved visualization of H_2O_2: the inflamed-to-normal contrast ratio was raised by 32% in Nile Red-doped FPOA NPs (4.1), compared to that of undoped FPOA NPs (3.1). This additional *in vivo* enhancement is unambiguously attributed to spectral tuning of the enhanced CL emission toward the biologically more transparent window, varifying the beneficial feature of FPOA NPs whose densely integrated nature facilitates intraparticle CL energy harvest to a low-energy dopant. Importantly, the red-tuned enhanced CL emission of FPOA NPs, though still in the visible region with a low degree of light penetration, is significantly brighter (8.2 times) than the NIR signal from FPOC NPs when observed through the biological thick specimen (Figure 7c). This brighter signal of FPOA NPs under the *in vivo* mimicking condition reveals that our approach based on the AEF dye/peroxalate dual integration is truly valid for amplifying the CL

imaging signals, offering a promising pathway to high-sensitivity disease diagnosis.

CONCLUSION

We have formulated a Pluronic-based nanoreactor system (FPOA NPs) for POCL, which is concentrated with AEF-active dye/peroxalate coaggregates. It turned out that the utilization of AEF-active dyes as a luminescent energy acceptor for POCL permitted the preparation of dye-concentrated nanoparticles having robust CL emission whose intensity can be cumulatively enhanced by increasing the dye loading. In addition to the signal enhancement effect by AEF, it was found that the dense nanointegration approach facilitates the intraparticle energy transfer from H_2O_2-reacted peroxalates to dye aggregates and further to a low-energy dopant to tune the spectrum toward the biologically transparent window. The enhanced and tunable CL allowed for the sensitive imaging of endogenous H_2O_2 produced during immune response and inflammation in cells and *in vivo*, validating our multimolecule integration strategy for the enhanced CL generation.

EXPERIMENTAL SECTION

Materials and Instrumentation. All chemical reagents were purchased from Aldrich and TCI and used as received. Chemical structures were identified by ^{1}H NMR (Varian unity plus 300) and elemental analysis performed on a CHNS-O analyzer (EA 1180, FISONS Instruments). Mass spectra were obtained by matrix-assisted laser desorption/ionization time-of-flight (MALDI-TOF) mass spectrometry (Voyager DE-STR, Applied Biosystems) using α-cyano-4-hydroxycinnamic acid in THF as a matrix. Particle size distribution of a nanoparticle dispersion in deionized water was determined at 25 °C by using a particle sizer (90Plus, Brookhaven Instruments Corporation). Transmission electron microscopic (TEM) images were obtained with a CM30 electron microscope (FEI/Philips) operated at 200 kV. For the TEM sample preparation, a drop of particle dispersion was dried on a 300-mesh copper grid coated with carbon and negatively stained with a 2 wt % uranyl acetate solution. Absorption and emission (PL and CL) spectra were acquired using a UV−visible spectrometer (Agilent 8453) and a fluorescence spectrophotometer (Hitachi F-7000, wavelength calibrated for excitation and emission), respectively. Relative fluorescence quantum yields (Φ_f) of BLSA in the aggregated and solution forms were determined using an ethanol solution of rhodamine B as a reference. For the acquisition of CL spectra, photoexcitation was not used. CL intensities were calculated from the area under each CL spectral curve or from the CL images of samples in 96-well plates, captured by an unfiltered 12-bit CCD camera (Kodak Image Station 4000MM, New Haven, CT) or an IVIS Spectrum imaging system (Caliper, USA).

Synthesis of 4-Vinylbenzyl Laurate. 4-Vinylbenzyl chloride (1 mL, 7.10 mmol) was added in small portions to a solution of lauric acid (1.70 g, 8.52 mmol) and potassium carbonate (1.18 g, 8.52 mmol) in dry DMF (10 mL). The reaction mixture was heated at 80 °C for overnight under magnetic stirring. After completion of reaction (as judged by thin-layer chromatography), the reaction mixture was poured into cold brine and the precipitate collected by filtration was washed with water to remove salts. The white precipitate was washed thoroughly with methanol and dried under vacuum to give a product pure enough for the next step. Yield 2.62 g (83%). ^{1}H NMR ($CDCl_3$, 300 MHz, ppm): δ 0.88 (t, J = 6.6 Hz, 6H), 1.25 (m, 16H), 1.64 (m, 2H), 2.35 (t, J = 7.6 Hz, 2H), 5.10 (s, 2H), 5.26 (d, J = 11.0 Hz, 1H), 5.75 (d, J = 17.6 Hz, 1H), 6.71 (q, J = 9.3 Hz, 1H), 7.31 (d, J = 8.1 Hz, 2H), 7.40 (d, J = 8.1 Hz, 2H). IR (KBr, cm^{-1}): 2920−2850 (C−H), 1735 (C═O), 1620 (C═C). Anal. Calcd for $C_{21}H_{32}O_2$: C, 79.70; H, 10.19; O, 10.11. Found: C, 79.1; H, 10.8; O, 10.1.

Synthesis of (4,4′-(1*E*,1′*E*)-2,2′-(Anthracene-9,10-diyl)bis(ethene-2,1-diyl) Bis(4,1-phenylene)) Bis(methylene) Didodecanoate (BLSA). A mixture of 4-vinylbenzyl laurate (300 mg, 0.95 mmol), 9,10-dibromoanthracene (127 mg, 0.38 mmol), $Pd(OAc)_2$ (4.3 mg, 0.019 mmol), tri-*o*-tolylphosphine (28.9 mg, 0.095 mmol), tributylamine (1.8 mL), and NMP (8 mL) was introduced into a pressure tube under argon atmosphere. The reaction mixture was heated for 1 day at 80 °C and poured into methanol after cooling. The filtered precipitate was thoroughly washed with methanol and purified by column chromatography on a silica gel. The impurities were removed using EA/*n*-hexane (1/10 by volume), and then the product was collected by eluting with 1/3. Yield 136 mg (44%). ^{1}H NMR ($CDCl_3$, 300 MHz, ppm): δ 0.88 (t, J = 6.5 Hz, 6H), 1.27 (m, 32H), 1.68 (m, 4H), 2.39 (t, J = 7.5 Hz, 4H), 5.18 (s, 4H), 6.94 (d, J = 16.6 Hz, 2H), 7.44−7.50 (m, 8H), 7.69 (d, J = 8.0, 4H), 7.95 (d, J = 16.5, 2H), 8.38 (q, J = 3.3, 4H). MS (MALDI): calcd for $C_{56}H_{70}O_4$, m/z = 806.53; found, m/z = 808.4. Anal. Calcd for $C_{56}H_{70}O_4$: C, 83.33; H, 8.74; O, 7.93. Found: C, 83.6; H, 9.5; O, 6.9.

Preparation of BLSA Nanoaggregates. An aqueous dispersion of BLSA nanoaggregates (5 μM) was prepared without surfactant for the study of AEF behavior. THF solution (50 μM, 1 mL) was added in one shot to 9 mL of water under sonication. A solution of the same concentration in THF (5 μM) was also prepared for comparative study.

Preparation of FPOA NPs. BLSA (1 mg) was homogeneously mixed with Pluronic F-127 (20 mg, Aldrich) and bis[3,4,6-trichloro-2-(pentyloxycarbonyl)phenyl] oxalate (CPPO, 0.5 mg, TCI) in THF (0.6 mL). After the solvent was evaporated by air flow, the dried mixture was mixed with Milli-Q water (1 mL) and then vigorously shaken to afford an aqueous dispersion of self-assembled FPOA NPs.

***In Vitro* Cell Labeling and Imaging.** *Mus musculus* RAW 264.7 macrophages were cultured in Dulbecco's modified Eagle medium with 10% FBS, 5 mM L-glutamine, and 5 μg/mL gentamicin in a humidified 5% CO_2 incubator at 37 °C. Cells were seeded onto 35 mm coverglass bottom dishes and allowed to grow until a confluence of 70%. Prior to experiments, cells were washed twice with PBS (pH 7.4) to remove the remnant growth medium and then incubated in a serum-free medium (1.8 mL) containing FPOA NPs (200 μL) for 10 min. For photoluminescence imaging, the labeled cells were then washed twice with PBS (pH 7.4) and directly imaged using a LEICA DMI3000B equipped with a Nuance FX multispectral imaging system (CRI, USA). For chemiluminescence imaging, cells were pretreated for 1 h in a serum-free medium (180 μL) containing 20 μL of phorbol 12-myristate 13-acetate (2 μg, Aldrich) to induce immune response or 20 μL of PBS for a normal control. The pretreated cells were labeled with FPOA nanoparticles as describe above and then imaged with an IVIS Spectrum imaging system (Caliper, USA).

***In Vivo* CL Imaging.** The animal studies have been approved by the animal care and use committee of Korea Institute of Science and Technology, and all handling of mice was performed in accordance with the institutional regulations. For arthritis model preparation, BALB/c mice (male, 5 weeks of age; Orient Bio Inc., Korea) were anaesthetized with intraperitoneal injection of 0.5% pentobarbital sodium (0.01 mL/g). Acute inflammation was induced by intra-articular injection of lipopolysaccharide (20 μL, 2 mg/mL in PBS, or 20 μL of PBS alone for a normal control) into the ankle of mice. *In vivo* CL imaging was done 48 h after LPS treatment with an IVIS Spectrum imaging system (Caliper, USA). Spectrally unmixed and unfiltered images were taken 1 min after intra-articular administration of nanoparticles (30 μL, 21.5 mg/mL).

Conflict of Interest: The authors declare no competing financial interest.

Acknowledgment. This work was supported by grants from the Korea Ministry of Education, Science and Technology (MEST)

(Nos. 2012-0001082 and 2012-0006061) and by the Intramural Research Program of KIST.

Supporting Information Available: Supplementary schemes and figures. This material is available free of charge *via* the Internet at http://pubs.acs.org.

REFERENCES AND NOTES

1. Giorgio, M.; Trinei, M.; Migliaccio, E.; Pelicci, P. G. Hydrogen Peroxide: A Metabolic By-Product or a Common Mediator of Ageing Signals? *Nat. Rev. Mol. Cell Biol.* **2007**, *8*, 722–728.
2. Zhang, K.; Kaufman, R. J. From Endoplasmic-Reticulum Stress to the Inflammatory Response. *Nature* **2008**, *454*, 455–462.
3. Lu, C.; Song, G.; Lin, J.-M. Reactive Oxygen Species and Their Chemiluminescence-Detection Methods. *Trends Anal. Chem.* **2006**, *25*, 985–995.
4. *Chemiluminescence in Analytical Chemistry*; Garcia-Campana, A. M., Baeyens, W. R. G., Eds; Marcel Dekker: New York, 2001.
5. Roda, A.; Guardigli, M.; Pasini, P.; Mirasoli, M.; Michelini, E.; Musiani, M. Bio- and Chemiluminescence Imaging in Analytical Chemistry. *Anal. Chim. Acta* **2005**, *541*, 25–36.
6. Lee, D.; Khaja, S.; Velasquez-Castano, J. C.; Dasari, M.; Sun, C.; Petros, J.; Taylor, W. R.; Murthy, N. *In Vivo* Imaging of Hydrogen Peroxide with Chemiluminescent Nanoparticles. *Nat. Mater.* **2007**, *6*, 765–769.
7. Lee, D.; Erigala, V. R.; Dasari, M.; Yu, J.; Dickson, R. M.; Murthy, N. Detection of Hydrogen Peroxide with Chemiluminescent Micelles. *Int. J. Nanomed.* **2008**, *3*, 471–476.
8. Dasari, M.; Lee, D.; Erigala, V. R.; Murthy, N. Chemiluminescent PEG-PCL Micelles for Imaging Hydrogen Peroxide. *J. Biomed. Mater. Res., Part A* **2009**, *89A*, 561–566.
9. Lim, C.-K.; Lee, Y.-D.; Na, J.; Oh, J. M.; Her, S.; Kim, K.; Choi, K.; Kim, S.; Kwon, I. C. Chemiluminescence-Generating Nanoreactor Formulation for Near-Infrared Imaging of Hydrogen Peroxide and Glucose Level *in Vivo*. *Adv. Funct. Mater.* **2010**, *20*, 2644–2648.
10. Birks, J. B. *Photophysics of Aromatic Molecules*; Wiley: London, 1970.
11. Luo, J.; Xie, Z.; Lam, J. W. Y.; Cheng, L.; Chen, H.; Qiu, C.; Kwok, H. S.; Zhan, X.; Liu, Y.; Zhu, D.; Tang, B. Z. Aggregation-Induced Emission of 1-Methyl-1,2,3,4,5-pentaphenylsilole. *Chem. Commun.* **2001**, 1740–1741.
12. Hong, Y.; Lam, J. W. Y.; Tang, B. Z. Aggregation-Induced Emission: Phenomenon, Mechanism and Applications. *Chem. Commun.* **2009**, 4332–4353.
13. An, B.-K.; Kwon, S.-K.; Jung, S.-D.; Park, S. Y. Enhanced Emission and Its Switching in Fluorescent Organic Nanoparticles. *J. Am. Chem. Soc.* **2002**, *124*, 14410–14415.
14. Xiao, D.; Xi, L.; Yang, W.; Fu, H.; Shuai, Z.; Fang, Y.; Yao, J. Size-Tunable Emission from 1,3-Diphenyl-5-(2-anthryl)-2-pyrazoline Nanoparticles. *J. Am. Chem. Soc.* **2003**, *125*, 6740–6745.
15. Yeh, H.-C.; Yeh, S.-J.; Chen, C.-T. Readily Synthesised Arylamino Fumaronitrile for Non-doped Red Organic Light-Emitting Diodes. *Chem. Commun.* **2003**, 2632–2633.
16. Palayangoda, S. S.; Cai, X.; Adhikari, R. M.; Neckers, D. C. Carbazole-Based Donor−Acceptor Compounds: Highly Fluorescent Organic Nanoparticles. *Org. Lett.* **2008**, *10*, 281–284.
17. An, B.-K.; Gihm, S. H.; Chung, J. W.; Park, C. R.; Kwon, S.-K.; Park, S. Y. Color-Tuned Highly Fluorescent Organic Nanowires/Nanofabrics: Easy Massive Fabrication and Molecular Structural Origin. *J. Am. Chem. Soc.* **2009**, *131*, 3950–3957.
18. Shimizu, M.; Takeda, Y.; Higashi, M.; Hiyama, T. 1,4-Bis(alkenyl)-2,5-dipiperidinobenzenes: Minimal Fluorophores Exhibiting Highly Efficient Emission in the Solid State. *Angew. Chem., Int. Ed.* **2009**, *48*, 3653–3656.
19. Kim, S.; Zheng, Q.; He, G. S.; Bharali, D. J.; Pudavar, H. E.; Baev, A.; Prasad, P. N. Aggregation-Enhanced Fluorescence and Two-Photon Absorption in Nanoaggregates of a 9,10-Bis[4′-(4″-aminostyryl)styryl]anthracene Derivative. *Adv. Funct. Mater.* **2006**, *16*, 2317–2323.
20. He, J.; Xu, B.; Chen, F.; Xia, H.; Li, K.; Ye, L.; Tian, W. Aggregation-Induced Emission in the Crystals of 9,10-Distyrylanthracene Derivatives: The Essential Role of Restricted Intramolecular Torsion. *J. Phys. Chem. C* **2009**, *113*, 9892–9899.
21. Kim, S.; Pudavar, H. E.; Bonoiu, A.; Prasad, P. N. Aggregation-Enhanced Fluorescence in Organically Modified Silica Nanoparticles: A Novel Approach toward High-Signal-Output Nanoprobes for Two-Photon Fluorescence Bioimaging. *Adv. Mater.* **2007**, *19*, 3791–3795.
22. Kim, S.; Huang, H.; Pudavar, H. E.; Cui, Y.; Prasad, P. N. Intraparticle Energy Transfer and Fluorescence Photoconversion in Nanoparticles: An Optical Highlighter Nanoprobe for Two-Photon Bioimaging. *Chem. Mater.* **2007**, *19*, 5650–5656.
23. Kim, S.; Ohulchanskyy, T. Y.; Pudavar, H. E.; Pandey, R. K.; Prasad, P. N. Organically Modified Silica Nanoparticles Co-encapsulating Photosensitizing Drug and Aggregation-Enhanced Two-Photon Absorbing Fluorescent Dye Aggregates for Two-Photon Photodynamic Therapy. *J. Am. Chem. Soc.* **2007**, *129*, 2669–2675.
24. Chan, C. P.-Y.; Haeussler, M.; Tang, B. Z.; Dong, Y.; Sin, K.-K.; Mak, W.-C.; Trau, D.; Seydack, M.; Renneberg, R. Silole Nanocrystals as Novel Biolabels. *J. Immunol. Methods* **2004**, *295*, 111–118.
25. Kim, H.-J.; Lee, J.; Kim, T.-H.; Lee, T. S.; Kim, J. Highly Emissive Self-Assembled Organic Nanoparticles Having Dual Color Capacity for Targeted Immunofluorescence Labeling. *Adv. Mater.* **2008**, *20*, 1117–1121.
26. Lim, C.-K.; Kim, S.; Kwon, I. C.; Ahn, C.-H.; Park, S. Y. Dye-Condensed Biopolymeric Hybrids: Chromophoric Aggregation and Self-Assembly toward Fluorescent Bionanoparticles for Near Infrared Bioimaging. *Chem. Mater.* **2009**, *21*, 5819–5825.
27. Thompson, R. B.; McBee, S. E. S. Peroxyoxalate Chemiluminescence in Microemulsions. *Langmuir* **1988**, *4*, 106–110.
28. Rauhut, M. M.; Bollyky, L. J.; Roberts, B. G.; Loy, M.; Whitman, R. H.; Iannotta, A. V.; Semsel, A. M.; Clarke, R. A. Chemiluminescence from Reactions of Electronegatively Substituted Aryl Oxalates with Hydrogen Peroxide and Fluorescent Compounds. *J. Am. Chem. Soc.* **1967**, *89*, 6515–6522.
29. Wrona, M.; Patel, K.; Wardman, P. Reactivity of 2′,7′-Dichlorodihydrofluorescein and Dihydrorhodamine 123 and Their Oxidized Forms toward Carbonate, Nitrogen Dioxide, and Hydroxyl Radicals. *Free Radical Biol. Med.* **2005**, *38*, 262–270.
30. Li, H.; Li, Q.; Wang, X.; Xu, K.; Chen, Z.; Gong, X.; Liu, X.; Tong, L.; Tang, B. Simultaneous Determination of Superoxide and Hydrogen Peroxide in Macrophage RAW 264.7 Cell Extracts by Microchip Electrophoresis with Laser-Induced Fluorescence Detection. *Anal. Chem.* **2009**, *81*, 2193–2198.
31. Weissleder, R.; Ntziachristos, V. Shedding Light onto Live Molecular Targets. *Nat. Med.* **2003**, *9*, 123.
32. Prasad, P. N. *Introduction to Biophotonics*; John Wiley & Sons: Hoboken, NJ, 2003.
33. Chen, W.-T.; Mahmood, U.; Weissleder, R.; Tung, C.-H. Arthritis Imaging Using a Near-Infrared Fluorescence Folate-Targeted Probe. *Arthritis Res. Ther.* **2005**, *7*, R310–R317.